Ocean bottom pressure records from the Cascadia array and short surface gravity waves

Charles Peureux, Fabrice Ardhuin

AGU PUBLICATIONS

JGR

Journal of Geophysical Research: Oceans

RESEARCH ARTICLE

10.1002/2015JC011580

Ocean bottom pressure records from the Cascadia array and short surface gravity waves

Charles Peureux[1] and Fabrice Ardhuin[1]

[1]Laboratoire d'Océanographie Physique et Spatiale, UMR6523 CNRS/Ifremer/UBO/IRD, Plouzané, France

Key Points:
- Ocean bottom pressure spectra from 1 to 7 Hz are well-defined functions of the wind speed.
- Their variability is interpreted in terms of the overlap integral of surface waves.
- The overlap integral is poorly modeled at acoustic frequencies greater than 0.4 Hz.

Correspondence to:
C. Peureux,
cpeureux@ifremer.fr

Citation:
Peureux, C., and F. Ardhuin (2016), Ocean bottom pressure records from the Cascadia array and short surface gravity waves, *J. Geophys. Res. Oceans*, *121*, 2862–2873, doi:10.1002/2015JC011580.

Received 17 DEC 2015
Accepted 8 MAR 2016
Accepted article online 15 MAR 2016
Published online 1 MAY 2016

Abstract The ocean bottom pressure records from eight stations of the Cascadia array are used to investigate the properties of short surface gravity waves with frequencies ranging from 0.2 to 5 Hz. It is found that the pressure spectrum at all sites is a well-defined function of the wind speed U_{10} and frequency f, with only a minor shift of a few dB from one site to another that can be attributed to variations in bottom properties. This observation can be combined with the theoretical prediction that the ocean bottom pressure spectrum is proportional to the surface gravity wave spectrum $E(f)$ squared, times the overlap integral $I(f)$ which is given by the directional wave spectrum at each frequency. This combination, using $E(f)$ estimated from modeled spectra or parametric spectra, yields an overlap integral $I(f)$ that is a function of the local wave age $f/f_{PM}=fU_{10}/0.13\,g$. This function is maximum for $f/f_{PM}=8$ and decreases by 10 dB for $f/f_{PM}=2$ and $f/f_{PM}=30$. This shape of $I(f)$ can be interpreted as a maximum width of the directional wave spectrum at $f/f_{PM}=8$, possibly equivalent to an isotropic directional spectrum, and a narrower directional distribution toward both the dominant low frequencies and the higher capillary-gravity wave frequencies.

1. Introduction

Ocean waves are sources of low magnitude but permanent seismic activity. *Duennebier et al.* [2012] showed that ocean bottom pressure spectra recorded in Hawaii vary systematically with surface winds over a wide frequency range, from 10 mHz to 10 kHz. While the frequencies above 1 kHz are related to bubbles produced by wave breaking [e.g., *Nan et al.*, 1990], the low frequency range below 0.4 Hz, with a power peak usually near 0.2 Hz, is now well understood [*Ardhuin and Herbers*, 2013] as a combination of acoustic-gravity modes, that dominate near the surface [*Cox and Jacobs*, 1989], and seismic pseudo-Rayleigh modes, that dominate at the bottom. The latter can be strongly modified by sediment properties [*Latham et al.*, 1967; *Ardhuin et al.*, 2013] with the possible excitation of shear modes in addition to the Rayleigh modes. *Ardhuin et al.* [2015] have shown that most energy at frequencies between 0.03 and 0.4 Hz is generated by surface gravity wave trains propagating in nearly opposite directions with similar frequency, giving rise to acoustic or seismic waves at twice this ocean wave frequency. This "double frequency mechanism" (hereinafter DFM) was first proposed by *Bernard* [1941] and later explained by *Longuet-Higgins* [1950] and *Hasselmann* [1963], with corrections for finite water depth given by *Ardhuin and Herbers* [2013]. The importance of the mechanical properties of the crust for the amplitude of the pressure in the water column was first studied by *Abramovici* [1968] as a generalization of the *Hasselmann* [1963] theory to a multilayer description of the solid Earth. This problem was also treated by *Gualtieri et al.* [2014] using normal mode theory. At a frequency of 0.2 Hz, the attenuation of seismic waves is relatively weak and the pseudo-Rayleigh waves can propagate over thousands of kilometers along the ocean crust interface, and are also recorded on land [*Stutzmann et al.*, 2012]. The DFM theory thus predicts that the seismic or acoustic power at frequency f_s is a function of the surface gravity wave spectrum at frequency $f=f_s/2$, proportional to $E^2(f)I(f)$ with:

$$I(f)=\int_0^{2\pi} E(f,\theta)E(f,\theta+\pi)d\theta/E^2(f) \tag{1}$$

$$E(f)=\int_0^{2\pi} E(f,\theta)d\theta \tag{2}$$

where $E(f,\theta)$ is the surface wave frequency-direction spectrum.

It is expected that the DFM also explains recorded signals at frequencies from 0.4 to 10 Hz, and this was particularly investigated by *Farrell and Munk* [2008, 2010] and *Duennebier et al.* [2012] using data from the H_2O

and ALOHA bottom observatories. Although no direct validation of the DFM theory has been shown at these frequencies, the extension of the theory to the short gravity (0.4–5 Hz), ultragravity (5–27.5 Hz), and capillary domains (>27.5 Hz) is straightforward by accounting for surface tension effects [*Brekhovskikh*, 1966]. There has been some disagreements on the importance of bottom effects (e.g., *Guralnik et al*. [2013], estimate an enhanced bottom spectral density by 2.3 dB relative to the case without bottom), and the interpretation of the measured spectra in terms of surface gravity wave properties. Earlier work by *McCreery and Duennebier* [1988], *Webb* [1992], and *McCreery* [1993] suggested that the pressure for frequencies between 1 and 5 Hz is saturated for wind speeds above $10\,\mathrm{m}\cdot\mathrm{s}^{-1}$, with a shape that was independent of the measurement location, near Wake Island or in other oceans. This universal saturated spectrum was called the Holu (Hawaiian for "deep ocean") spectrum by *McCreery and Duennebier* [1988]. This saturation is expected to correspond to the saturation of the surface elevation spectrum $E(f)$ [*Phillips*, 1958], and a constant value of $I(f)$. Given the poor knowledge of short surface waves directional properties, the investigation of ocean acoustic spectra offers an interesting complement to satellite-based radar back scatter and radiometry, helping to constrain the shape of the directional spectrum of short waves.

The recent analysis by *Gimbert and Tsai* [2015] suggests that the overlap integral could be a function of the variability of the wind speed near the measurement site, presumably because more variable winds generally lead to broader directional distributions and thus larger values of $I(f)$. They also estimate a very low value for I, around -28 dB, from the ratio of a predicted microseismic power recorded on land and $E^2(f)$. However, their model ignores propagation effects from ocean to land, so that the absolute value of $I(f)$ they estimate is not reliable. The general problem of deep acoustic data or microseisms measured on land is that there are unknown frequency-dependent propagation factors that make it impossible to estimate the absolute value of I. Only near-surface measurements [e.g., *Cox and Jacobs*, 1989; *Ardhuin et al*., 2013] are independent of such factors because they are dominated by the evanescent acoustic-gravity modes, and contain little energy from the bottom-affected Rayleigh or shear modes, and direct estimates of $I(f)$ are now possible from stereo-video imagery of the sea surface [*Leckler et al*., 2015].

Duennebier et al. [2012] confirmed that the spectra averaged as a function of wind speed are indeed saturated between 2 and 3 Hz but still increase for both lower and higher frequencies. *Farrell and Munk* [2010] have further described in detail the variability below 5 Hz with "busts" in the acoustic power when the wind speed drops below $6\,\mathrm{m}\cdot\mathrm{s}^{-1}$, and "booms" above 5 Hz when the wind speed exceeds $6\,\mathrm{m}\cdot\mathrm{s}^{-1}$. These behaviors, combined with a very weak dependence of $E(f)$ on the wind speed [*Yurovskaya et al*., 2013], suggest that most of the variability in the acoustic power at the ocean bottom can be interpreted as a variability of $I(f)$.

Here we use the opportunity of the ongoing Cascadia array initiative [*Toomey et al*., 2014], on the North-East Pacific margin, to investigate the generality of the *Duennebier et al*. [2012] study in a different regime of ocean waves, and we particularly describe the variability of the ocean bottom acoustic power at frequencies between 0.5 and 10 Hz. The data are described in section 2. The link between ocean bottom acoustic noise and its surface sources is illustrated in section 3. In section 4, the noise around 1 Hz is interpreted in terms of directional properties of short surface waves. Conclusions are presented in section 5.

2. Data and Processing

We study ocean bottom differential pressure gauges and seismometer data from 8 stations in the southern part of the Cascadia array (Figure 1). We mainly focus on the pressure data (BDH channel). The length of records varies from station to station, between 2 and 9 months. The diversity of water depths (3215–107 m) and locations provides an interesting sampling of possible acoustic conditions. The data from this network named 7-D were downloaded from the Incorporated Research Institutions for Seismology (IRIS) website. The raw 50 Hz sampled data were processed into 1024 s long half-overlapping windows. In each window, the signal was detrended, multiplied by a Hann window, and Fourier transformed, providing spectra that were averaged over 3 h records with a 0.77 mHz frequency resolution using the Welsh method. The power spectral densities were corrected for the instrument response using the calibrations provided by IRIS. Smoothing the spectra over frequencies using a 20 points moving average below 0.5 Hz and 100 points above provides spectral estimates with 840 and 4200 degrees of freedom, for which we expect a random error of 10% and 5%, respectively.

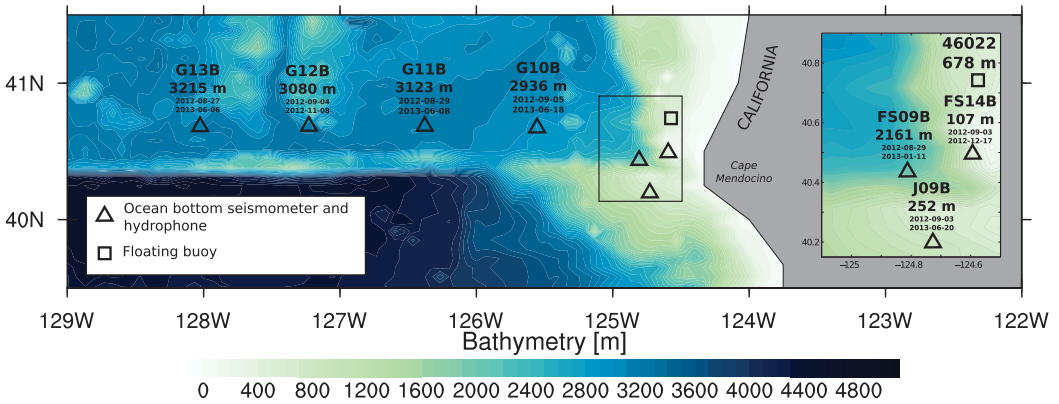

Figure 1. Cascadia array bathymetry (ETOPO2) and station locations with instrument depths and analyzed record start and end dates.

The bottom pressure spectrum F_p as a function of the acoustic frequency f_s is expected to be related to the surface gravity wave spectrum by:

$$F_p(f_s) = \gamma(f_s) E^2(f) I(f) \tag{3}$$

where E and I are local surface wave properties. The noise generation theory we use to calculate the transfer function γ is detailed in the Appendix A. Other theoretical expressions that give different values of γ can be found in *Farrell and Munk* [2010]. In order to analyze data spanning several orders of magnitude, we will hereinafter express spectra in dB relative to 1 $Pa^2 \cdot Hz^{-1}$, namely $F_{dB} = 10\log_{10}(F_p)$ with F_p in $Pa^2 \cdot Hz^{-1}$.

3. Spectral Shapes and Variability With Wind and Wave Parameters

The medians of $F_p(f_s)$ are presented on Figure 2. The pressure field is a combination of seismic waves, which vary like $\sin(lz)$ over the vertical z, where $l = \sqrt{(2\pi f_s)^2/\alpha_w^2 - k^2}$ and surface gravity waves, which vary like $\cosh(kz + kH)$ and thus decay exponentially over a scale that is the wavelength $L = 2\pi/k$. The strong depth dependence of the spectral peak around 0.06 Hz shows that these frequencies are dominated by gravity waves. They are barely detectable in 250 m depth (station J09B), where surface gravity waves with $f = 0.06$ Hz have a wavelength $L \simeq g/(2\pi f^2) \simeq 430$ m. In deeper water, the only gravity waves that can be measured at the bottom are in the infragravity wave band ($f < 0.03$ Hz) [*Webb*, 1992]. The secondary peak has a very weak depth dependence as expected from DFM theory, which makes it the dominant noise source at the ocean bottom in deep water. The f^{-6} slope of the pressure spectrum in the range $0.3 < f_s < 4$ Hz is the same as found by *Duennebier et al.* [2012] for low wind speeds.

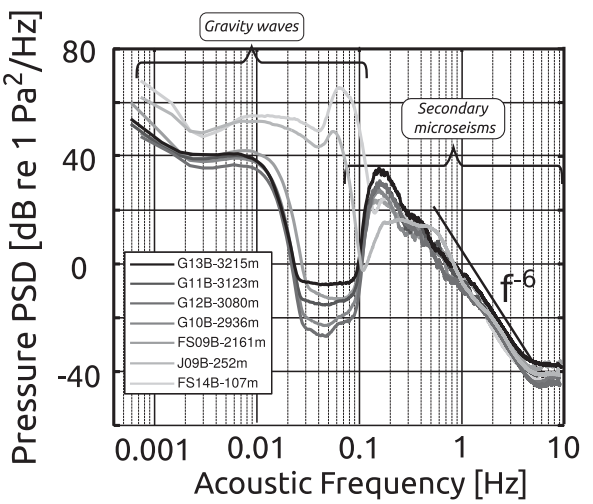

Figure 2. Median bottom pressure spectra at the stations studied.

F_p in dB is then correlated with the logarithm of our modeled significant wave height H_s and with the surface wind speed U_{10} provided by ECMWF (Figure 3), but restricted to events for which $U_{10} < 5\,m \cdot s^{-1}$. The wind speed field is the same which was used as input for our numerical ocean wave modeling (see Appendix A). These two variables are output on top of the instrument. As in *Farrell and Munk* [2010], the wind speed range 0 to $5\,m \cdot s^{-1}$ corresponds to a linear increase of the noise level (measured in dB) with U_{10} for frequencies $0.5\,Hz < f_s < 3\,Hz$ approximately. These correlations delineate

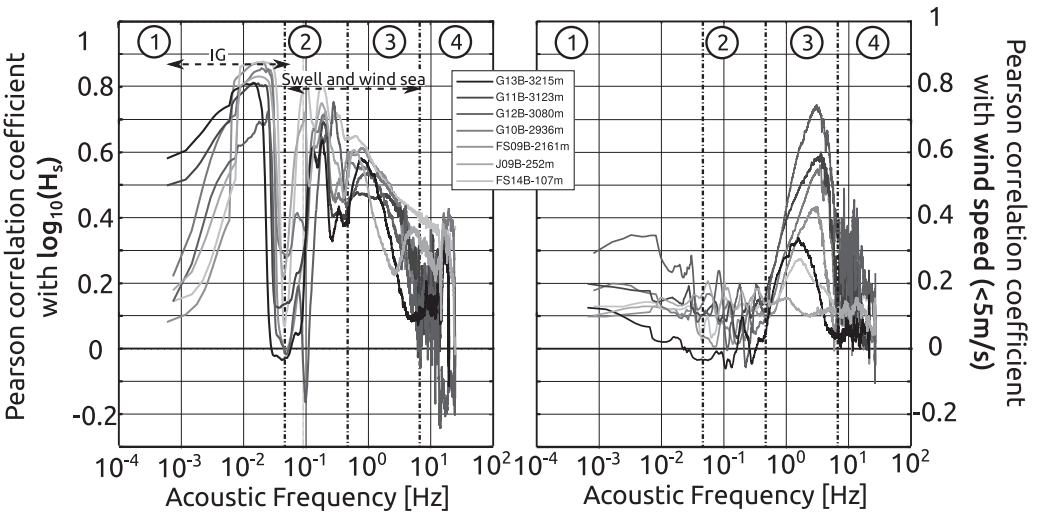

Figure 3. Pearson correlation coefficient as a function of acoustic frequency f_s (left) between $\log_{10}(F_p(f_s))$ and $\log_{10}(H_s)$ and (right) between $\log_{10}(F_p(f_s))$ and $U_{10} < 5\,\mathrm{m}\cdot\mathrm{s}^{-1}$ at the stations studied. See *Ardhuin et al.* [2010] for coefficient definitions.

three regions in the frequency domain, with definitions that differ from *Duennebier et al.* [2012]. Region 1 corresponds to infragravity (IG) waves and exhibits a strong correlation with H_s. This is consistent with the known sources of IG waves for this area that are dominantly coming from the nearby U.S. West Coast [*Ardhuin et al.*, 2013; *Rawat et al.*, 2014; *Neale et al.*, 2015]. The correlation with surface wind speed is very low, because IG waves are generated by long-period swells hitting the shoreline, which are themselves often generated by remote winds. Region 2 contains primarily generated noise up to approximately 0.2 Hz and DFM noise above. The correlation coefficient is less around the secondary peak than around the primary peak. From DFM theory, the secondary noise is less correlated with $H_s \simeq 4\sqrt{E(f)\Delta f_p}$, where f_p is the peak frequency, at which the spectral density is maximum, and Δf_p is the spectral width around the peak, than with $4\sqrt{E^2(f_p)I(f_p)\Delta f_p}$. Above 0.4 Hz, in region 3, the bottom pressure is strongly correlated to the local wind speed, due to the faster response of short waves to a change of wind speed. This distinction between short and long double-frequency microseisms has already been made in *Bromirski et al.* [2005], with a transition at 0.22 Hz. As a remarkable fact, the correlation with surface wind speed increases when frequency increases up to about 3 Hz, before sinking sharply at higher frequencies. This reduction in correlation goes with the transition from "busts" in region 3 to "booms" at higher frequencies in region 4, as shown in Figure 4. Indeed, at 4 Hz, the acoustic power is nearly constant, and only increases for rare and high wind speeds at higher frequencies, giving a weak correlation when the full range of wind speeds is considered. Hereinafter we will focus on the region 3 of spectra in deep water.

4. Interpretation of Acoustic Spectra Around 1 Hz

In this frequency range, because spectra are similar for all stations, we chose to present results for station G10B only.

4.1. Use of a Numerical Wave Model

As detailed in the Appendix A, the acoustic spectrum should be the incoherent sum of all acoustic waves generated by surface gravity waves. We use our global ocean wave model to estimate directional wave spectra every 3 h on a regular grid, from ocean surface winds provided by ECMWF. Using equation (3), this model provides us estimates of the bottom DFM pressure spectrum. One key parameter in the model is the quality factor Q which encompasses all scattering and 3-D propagation effects, proportional to $\exp(-2\pi f_s\Delta/(UQ))$, see Appendix A, equation (A5). We used a frequency-dependent quality factor Q inspired from *Ardhuin et al.* [2013] (see Table 2), which approaches $Q = 600$ at high frequencies. It was estimated by maximizing the correlation between the observed acoustic power and our model. A better accuracy on the value of Q can be reached following a method described in *Stutzmann et al.* [2012]. The

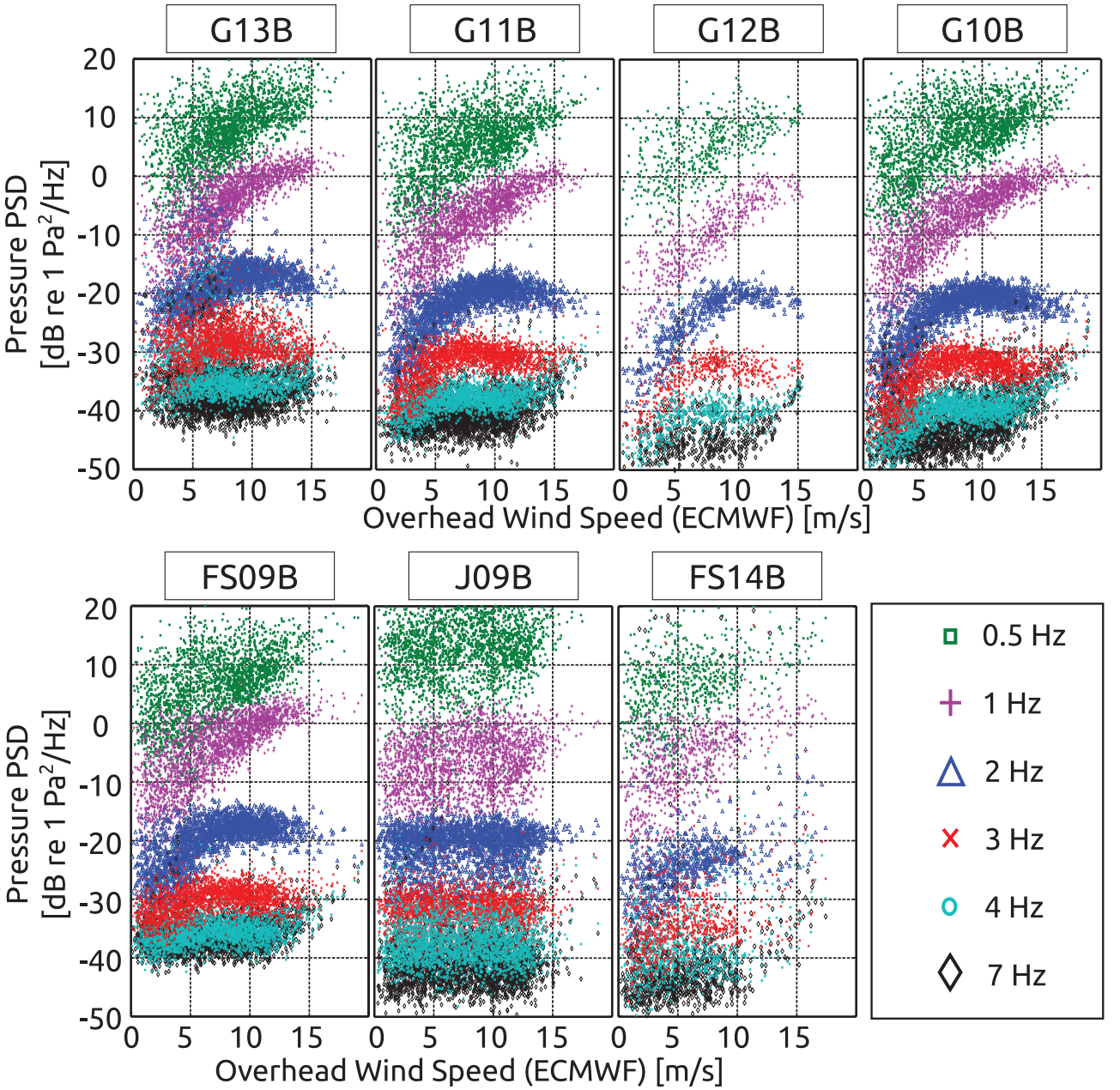

Figure 4. Bottom pressure 3 hourly averaged noise level scatterplots at the stations studied (deepest to shallowest, from left to right) plotted against U_{10} (ECMWF), or Holu spectra.

Rayleigh group speed is $U \simeq 1.5\,\mathrm{km} \cdot \mathrm{s}^{-1}$, given by the theoretical response of a water layer over an elastic half-space, so that 1 Hz seismic waves lose half of their power over 100 km of propagation. This distance is typically less than the correlation distance of the wind and wavefields, so that we can assume the waves to be homogeneous on that scale, making the acoustic spectrum directly proportional to the local wave spectrum and overlap integral, as given by equation (3).

Model results are presented on Figure 5 for the bottom pressure at station G10B. Results are similar using seismometer data. The modeled RMS pressure is in good qualitative agreement with observations for seismic frequencies up to 0.4 Hz, with a good reproduction of the temporal variability. The magnitude of predicted acoustic power has a frequency-dependent bias which can be partly attributed to the simplified treatment of the oceanic crust and sediments as a homogeneous elastic half-space. In particular, for f_s around 0.2–0.3 Hz, a small error in the crust properties can shift the resonant organ pipe modes, explaining the discrepancies between model and observations [*Ardhuin et al.*, 2013]. Above 0.4 Hz, the model error is a

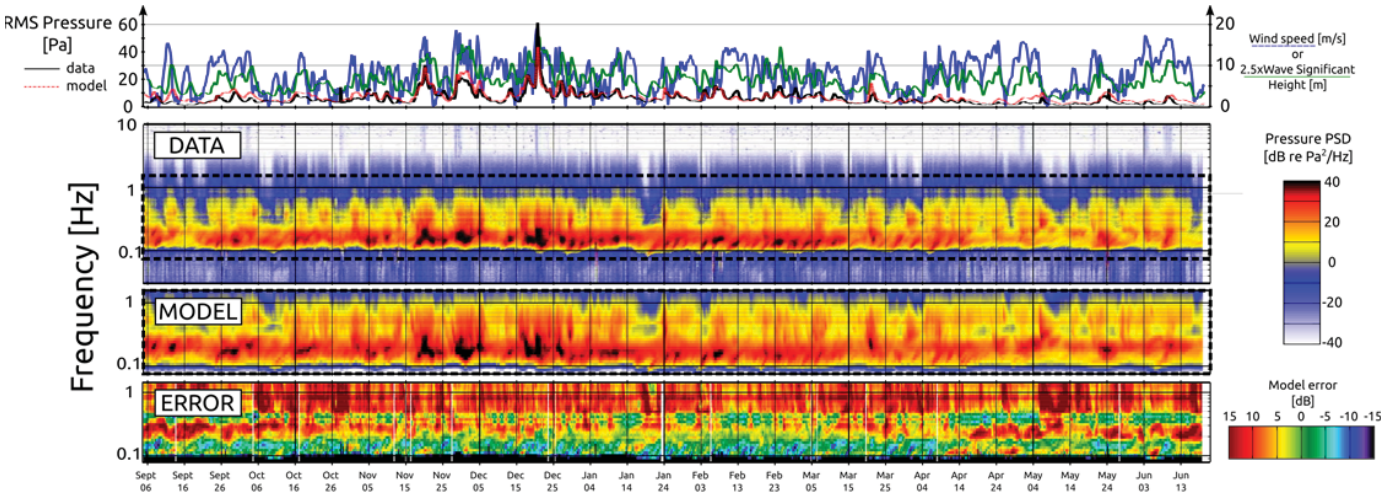

Figure 5. Bottom pressure spectrograms at station G10B. (top) RMS pressure $p_{RMS}=\sqrt{\int_{0.04\,Hz}^{10\,Hz} F_p df}$ and sea state variables. (bottom) Spectrograms of observed and modeled acoustic noise at station G10B, and associated error $\Delta_{dB}=10\log_{10}\left(F_p^{model}\right)-10\log_{10}\left(F_p^{data}\right)$.

decreasing function of surface wind speed (see Figure 6), with a positive bias of the order 10 dB associated with an overestimation of the quality factor. Reaching such an accuracy on the quality factor is beyond the scope of the present paper.

Errors for $f_s > 0.4$ Hz are not a simple shift by a few dB, as shown in Figure 7. Even with errors in the elastic model, the scatterplot of F_p (y axis) in dB as a function of $E^2(f)I(f)$, both expressed in dB, should be a straight line with slope 1 and y intercept $\gamma(f_s)$ (regression plot). Deviations from that behavior are caused by errors in the wave model, coming from poor estimates of $E(f)$ or $I(f)$. As previously found by *Ardhuin et al.* [2013], we have a higher correlation of the acoustic power with $E^2(f)$ than with $E^2(f)I(f)$ for $f_s > 0.6$ Hz. Given that wave models have never been properly tested for $I(f)$ at these frequencies, whereas $E(f)$ agrees with measurements at nearby buoys for f up to 0.5 Hz corresponding to $f_s = 2f = 1$ Hz, it follows that the model is unable to reproduce the variability of $I(f)$, which is better taken constant. At 0.4 Hz (40 m wavelength surface waves), the correlation is higher with $E^2 I$ compared to E^2, meaning that the model has some skills in predicting $I(f)$ for $f = 0.2$ Hz, as already found by *Ardhuin et al.* [2013]. It was already noted that the evaluation of the directional properties of these intermediate wind-waves strongly depends on the choice of the wave model parameterization for wave generation and dissipation [*Ardhuin et al.*, 2011, 2013].

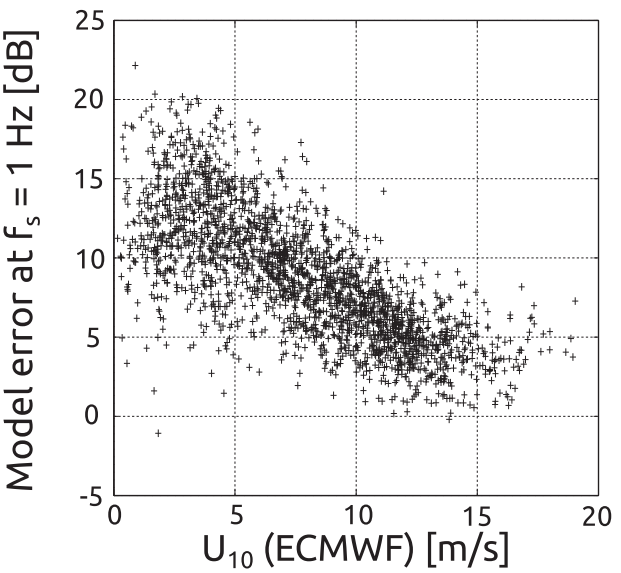

Figure 6. Model error Δ_{dB} (see Figure 5 for definition) at station G10B at acoustic frequency $f_s = 1$ Hz as a function of surface wind speed.

At $f_s = 0.7$ or 1 Hz, $I(f)$ is underestimated for high winds, and overestimated for low winds. In other words, high wind speed modeled directional spectra of short waves are too narrow, and too broad at low wind speeds, with an error of the order 10 dB.

4.2. Estimation of the Overlap Integral

As described in *McCreery* [1993], the growth of acoustic power with wind speed, $2\,dB/(m \cdot s^{-1})$, and a saturation stage past a wind of about $5-6\,m \cdot s^{-1}$,

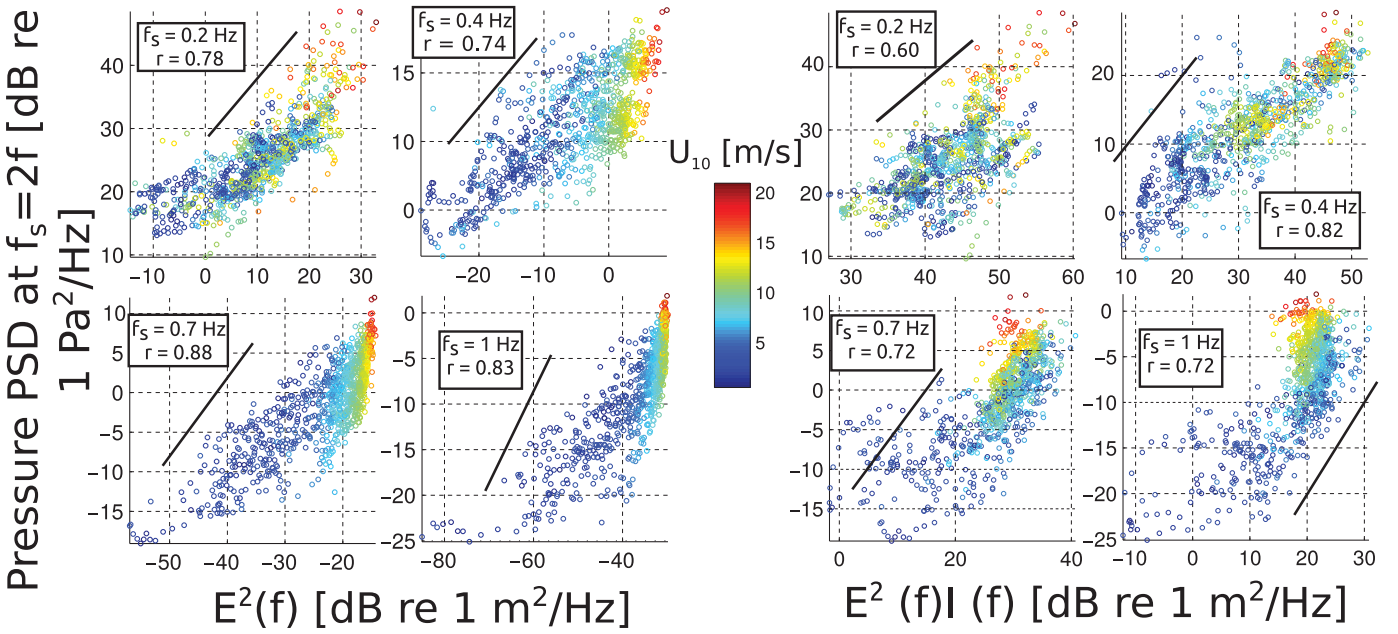

Figure 7. Bottom pressure noise level at station G10B as a function of (left) $E^2(f)$ and (right) $E^2(f)I(f)$ above the instruments as computed by our numerical wave model at several acoustic frequencies f_s. Pearson correlation coefficients r are printed in the captions.

suggest a particular shape of the directional surface wave spectrum when the acoustic spectrum saturates. A transition to another behavior at high wind speeds occurs at 3 Hz, where the acoustic power slightly decreases before growing again with increasing wind speed. This behavior has not been described before, possibly because it only occurs at wind speeds above 15 $m \cdot s^{-1}$, that are not very frequent. This behavior can be related to the decrease of the correlation coefficient above 3 Hz on Figure 7. The noise level at a given frequency is almost independent of station depth, although discrepancies are probably due to different sediment floor compositions [*Abramovici*, 1968] or calibration errors. Large vertical scatters at FS14B can be related to its proximity to ship traffic.

4.3. Parametrization of the Overlap Integral

Given a reliable estimate of the wave spectrum $E(f)$, an overlap integral $I(f)$ can be estimated from the pressure and crust vertical velocity spectra, especially at high frequencies for which equation (3) applies, namely:

$$I(f) = \frac{F_p(f_s)}{\gamma(f_s)E^2(f)} \tag{4}$$

We use the *Elfouhaily et al*. [1997] spectrum parametrization from the wind speed and wave age, instead of the one derived from our numerical wave model, because the latter tends to be biased high for $f > 0.4$ Hz [*Rascle and Ardhuin*, 2013]. For simplicity, we assume a fully developed sea state, for which the peak wave's frequency is given by *Pierson and Moskowitz* [1964]:

$$f_{PM} = 0.13g/U_{10} \tag{5}$$

Corrections for younger wave ages due to finite fetch or duration effects only introduce minor differences in the frequencies investigated here ($f > f_{PM}$), much less than the actual scatter of noise level at given frequency and wind speed. The Elfouhaily spectrum was converted from a wave number spectrum $E(k)$ to a frequency spectrum $E(f)$ assuming the linear dispersion relation:

$$E(f) = \frac{2\pi}{c_g(k)}E(k) \tag{6}$$

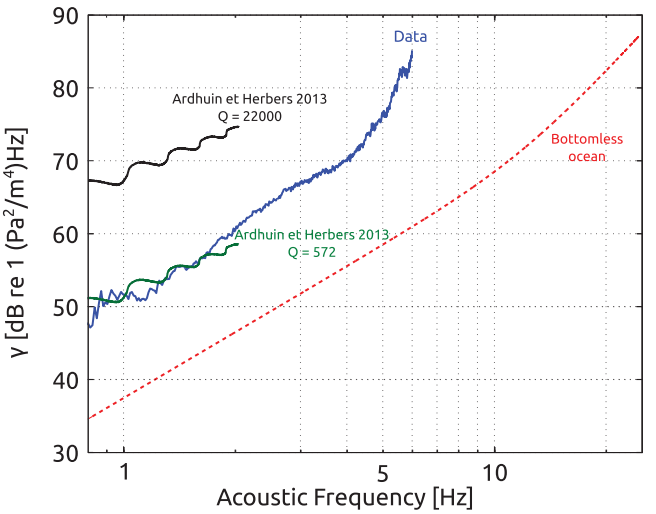

Figure 8. Several estimates of γ as a function of acoustic frequency f_s, from the data (blue solid line) using equation (9), from the bottomless ocean theory (red dashed line) using equation (11), and from equation (A7) for $Q = 22{,}000$ or $L_{att} = 2\pi R_e$ at $f_s = 1$ Hz (black solid line) and $Q = 572$ (green solid line).

where $c_g = \partial\sigma/\partial k$ is the group speed of surface waves, obtained by differentiation of the dispersion relation:

$$\sigma^2 = gk + Tk^3 \tag{7}$$

where $T = g/k_m^2$, and $k_m = 370\,\mathrm{rad}\cdot\mathrm{m}^{-1}$ is the transition wave number from gravity to capillary waves for clean water [*Elfouhaily et al.*, 1997]. This linear approximation holds up to $f = 4f_{PM}$, which gives $f_s = 1.4$ Hz for the average wind speed of $7\,\mathrm{m}\cdot\mathrm{s}^{-1}$. The effects of long wave orbital currents on shorter waves [*Longuet-Higgins and Stewart*, 1961] are neglected here, but they could represent a less than 1 dB correction according to *Korotkevich* [2008]. The empirical overlap integral (4) can be plotted as a function of:

$$\frac{f}{f_{\mathrm{PM}}} = \sqrt{\frac{k}{k_{PM}}} = 1.2\frac{U_{10}}{C} \tag{8}$$

where C is the surface wave phase speed (see equation (5)). This parametrization is almost the same as in [*Duennebier et al.*, 2012] (without the factor 1.2) and corresponds to the square root of the $\frac{k}{k_p}$ parameter used in Elfouhaily spectrum in the case of a fully developed sea.

As the seismic propagation effects are not well known, we need to correct them. For this, we will now assume that the particular shape of the directional wave spectrum when the acoustic saturates corresponds to $I(f_s) = 1/(2\pi) = -8$ dB. This particular value corresponds to an isotropic spectrum, but it can also correspond to a broad bimodal directional distribution, as in *Leckler et al.* [2015]. This assumption gives:

$$\log\left[\gamma(f_s)\right] \simeq \log(2\pi) + \overline{\log\left[\frac{F_p(f_s)}{E^2(f)}\right]}_{\frac{f}{f_{\mathrm{PM}}}\simeq 6} \tag{9}$$

where $\overline{(\ldots)}_{\frac{f}{f_{\mathrm{PM}}}\simeq 6}$ stands for an average of samples for which $5.5 < \frac{f}{f_{\mathrm{PM}}} < 6.5$. In other words, it is assumed that the contribution of the overlap integral to the noise at frequency f_s is maximum when U_{10} is approximately equal to 5 times the phase velocity of the ocean surface wave at frequency $f = f_s/2$ and is equivalent to the one of an isotropic wavefield.

We note that $I = -28$ dB proposed by *Gimbert and Tsai* [2015] is too low compared to recent measurements [*Leckler et al.*, 2015], and the 20 dB difference could be caused by propagation effects [e.g., *Gualtieri et al.*, 2015] that they did not take into account. Noise generation theory predicts [*Ardhuin et al.*, 2013]:

$$\gamma(f_s) = 32\pi^6 \frac{\rho_w^4 g^2 f_s^6}{\beta_c^5 \rho_s^2} L_{\mathrm{att}} \sum_j \left[\frac{\tan(l_j h)}{l_j}\right]^2 c_j^2(f_s) \tag{10}$$

where L_{att} is the effective attenuation length (see Appendix A). Additionally, for gravity waves without surface tension in a bottomless ocean [*Guralnik et al.*, 2013], we would have:

$$\gamma^b(f_s) = \frac{\rho_w^2 \omega_s^5 c_g(f) C(f)}{4\alpha_w^2} \tag{11}$$

This expression accounts for capillary effects and corresponds to the expression given by *Hughes* [1976] (see *Farrell and Munk* [2013] appendix for a review). An estimate of γ at station G10B above 0.8 Hz from the data is provided on Figure 8. Theoretical values are overlaid. The frequency dependence matches the predictions. The bottomless ocean model underestimates the noise by about 10–15 dB. As the acoustic energy

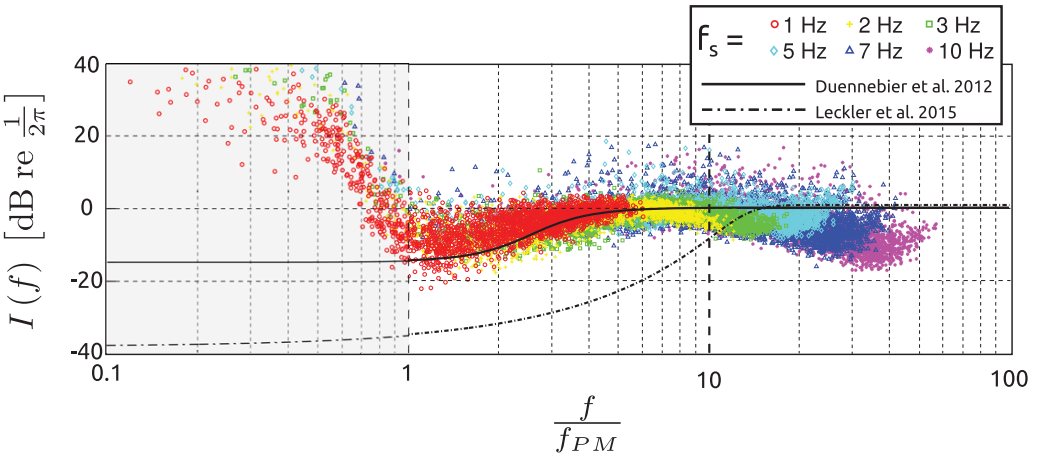

Figure 9. Overlap integral estimation from pressure data at station G10B (dB relative to saturation level $I=(2\pi)^{-1} \simeq -8$; dB) as a function of $\frac{f}{f_{PM}}$ (see equation (5)) at several surface wave frequencies. Previous estimates of the overlap integral are also displayed, based on acoustic noise data [*Duennebier et al*., 2012] (solid line) and stereo-video data [*Leckler et al*., 2015] (dash-dotted line).

is trapped in the wave guide consisting of the upper crust and water, the noise power is proportional to Q, as a result of a balance between dissipation and seismic noise generation.

These values of γ can now be used in (4) together with Elfouhaily spectrum, and this method provides an estimate of $I(f)$, as shown on Figure 9, that is independent of the station chosen. The previous estimate from bottom acoustic data by *Duennebier et al*. [2012] and from stereo-video measurements of the surface elevation by *Leckler et al*. [2015] are plotted for comparison. For f/f_{PM} between 1 and 4, the value of *Duennebier et al*. [2012] is lower by a few dB, whereas it is higher at higher frequencies. *Leckler et al*. [2015] measured waves with $f_p = 0.33$ Hz and f_{PM} ranging from 0.15 to 0.75 Hz approximately. The difference between *Leckler et al*. [2015] and the other two curves could be caused by an unknown difference in wave properties, or our assumption of a saturated value of $I(f)$ at $1/(2\pi)$.

For $\frac{f}{f_{PM}} > 8-10$, we find that the overlap integral starts decreasing for high values of $\frac{f}{f_{PM}}$, which is an indication for an increase of the directionality of the short wavefield in this range. At frequencies $f > 6$ Hz, the overlap integral increases again. This broadening or narrowing of the directional spectrum is consistent with Elfouhaily's ratio of upwind to crosswind energy which provides a different estimate of the width of the directional spectrum [*Elfouhaily et al*., 1997, equations (48) and (57)]. One interpretation of this match is that the double-frequency wave-wave interactions at high frequencies mostly occur between waves traveling in the crosswind direction, as supported by the video data of *Leckler et al*. [2015]. At these angles, waves are possibly generated by long wave breaking [*Kudryavtsev et al*., 2005] or other mechanisms that are not taken into account in our numerical wave model.

5. Conclusions

Ocean bottom pressure spectra in the frequency band 0.2–10 Hz contain information on the energy of surface gravity waves traveling in opposite directions, with half the frequency of the bottom pressure, giving an interesting constraint on the poorly known directional wave properties. The evolution of this signal is in good agreement with our knowledge of wave spectra up to acoustic frequencies of 0.4 Hz, as represented in numerical wave models. Above this limit, errors have been found to mainly originate from an underestimation of the overlap integral, $I(f)$, at high winds and an overestimation at low winds in numerical models.

Assuming that the saturation that is found for the acoustic spectrum at frequencies from 1 to 7 Hz corresponds to the same value of $I(f)=1/(2\pi)$, which is the value for an isotropic spectrum, we find that, for all frequencies, this saturation occurs at 5 times the Pierson-Moskowitz frequency f_{PM}, and that the variability of $I(f)$ is a well-defined function of f/f_{PM}. Future work will be needed to remove the need for this assumption, and directly measure $I(f)$ without contamination from unknown bottom properties. This can probably be achieved by surface slope measurements, or the measurement of acoustic power closer to the sea surface, where it is dominated by acoustic-gravity modes [*Cox and Jacobs*, 1989].

Table 1. Model Validation at Buoy 46022[a]

	H_s (WW3)	U_{10} (ECMWF)
Normalized root-mean-square error	14%	22%
Normalized bias	5%	5%
Pearson correlation coefficient	0.94	0.91

[a]Refere to *Ardhuin et al.* [2010, section4] for coefficient definitions.

Appendix A: Double Frequency Noise Modeling

A1. Numerical Wave Modeling

Ocean wave frequency-directional spectra $E(f,\theta)$ are evaluated by means of our state-of-the-art numerical spectral wave model, based on the WAVEWATCH® III (WW3) modeling framework [*Tolman*, 2014]. Parameterizations described in *Ardhuin et al.* [2010] forced by wind speeds from ECMWF operational analysis [*Bidlot et al.*, 2007] have been adjusted to produce accurate wave heights [*Rascle and Ardhuin*, 2013]. The model produces wave spectra every 3 h at each node of a global grid with a regular resolution of 0.5° in latitude and longitude for frequencies ranging from 0.037 to 0.72 Hz. Shoreline reflections are taken into account following *Ardhuin and Roland* [2012]. The wind and ocean wave models are validated in our region of interest at NDBC buoy 46022 (see Figure 1 and Table 1), and was validated globally using satellite altimeter data [*Rascle and Ardhuin*, 2013].

A2. Noise Generation Model—Coupling With the Solid Earth

We use the noise generation model of *Hasselmann* [1963] which applies to a homogeneous water column and bottom, with corrections for finite water depths in *Ardhuin and Herbers* [2013]. Both of these papers give the simplified expression for a stationary source field, which is appropriate for our frequency range of interest because the attenuation limits the effective radiation distance from the source to a few thousands of kilometers, which is reached in under 1 h, a time interval over which the sea state can be considered constant. The main results are summarized in the following. First, for ocean waves in deep enough water [*Ardhuin and Herbers*, 2013] and at $\mathbf{K} \simeq \mathbf{0}$ (i.e., wave numbers much smaller than the ones of ocean waves), the double-frequency motion at the sea surface is equivalent to a surface pressure field that is a function of $E(f)$ and $I(f)$ given by (2)–(1) from the modeled ocean wave spectrum $E(f,\theta)$. This equivalent DFM pressure has a power spectrum:

$$F_{p,\mathrm{surf}}(\mathbf{K} \simeq \mathbf{0}, f_s) = \rho_w^2 g^2 f E^2(f) I(f) \tag{A1}$$

where $f = \frac{f_s}{2}$ is the frequency of surface waves, g is the vertical acceleration due to gravity, and ρ_w is the density of seawater.

This pressure field is the source of a seismo-acoustic wavefield which increases by the amount $S_{DF,j}$ per unit distance of propagation across the source area [*Ardhuin and Herbers*, 2013, equation (4.33)]:

$$S_{DF,j}(f_s) = \frac{4\pi^2 f_s c_j^2}{\beta_c^5 \rho_c^2} F_{p,\mathrm{surf}}(\mathbf{K} \simeq \mathbf{0}, f_s) \tag{A2}$$

where c_j is the site effect coefficient of mode j as introduced by *Longuet-Higgins* [1950] and computed here using *Ardhuin and Herbers* [2013, equations ((4).34) and (4.26)]. c_j is a function of the crust shear wave speed β_c, compression speed α_c, and density ρ_c as well as the water depth, density, and sound speed of the seawater. Model parameters for station G10B are gathered in Table 2.

At a given location and seismo-acoustic frequency f_s, the power spectrum F_v of the crust vertical velocity is made of the contributions of modes j from each elementary ocean area dS at the mean sea surface ∂V_e:

$$F_v(f_s) = (2\pi f_s)^2 \int_{\partial V_e} dS \sum_{j=1}^{\infty} S_{DF,j}(f_s) \frac{e^{-\alpha_j(f_s)\Delta R_e}}{R_e \sin\Delta} \tag{A3}$$

with SI unit of $(\mathrm{m/s})^2/\mathrm{Hz}$, where R_e is the Earth's radius, Δ is the spherical distance (angle at the center of the Earth) between the source area dS and the observation location, α_j is the attenuation coefficient, which is parameterized as a function of the group speed U_j of pseudo-Rayleigh waves and a quality factor Q_j:

$$\alpha_j(f_s) = \frac{2\pi f_s}{U_j Q_j(f_s)} \tag{A4}$$

Table 2. Model Parameters Used for Noise Modeling at Station G10B[a]

Variable	Meaning	Value
ρ_w	Seawater density	1.0×10^3 kg · m^{-3}
α_w	Compression wave velocity in water	1.5×10^3 m · s^{-1}
ρ_c	Crust density	2.6×10^3 kg · m^{-3}
α_c	Compression wave velocity in the crust	5.8×10^3 m · s^{-1}
β_c	Shear wave velocity in the crust	3.2×10^3 m · s^{-1}
$Q(f_s)$	Seismic wave quality factor	$600\{1+[1-\tanh[15(f_s-0.14\,\text{Hz})]]\}$

[a]The mathematical shape of the quality factor is inspired from *Ardhuin et al.* [2013]. The more important attenuation of seismic waves with frequency has been taken into account by reducing Q toward high frequencies.

From the theory, we can convert the bottom velocity into a bottom pressure p, with a power spectrum given by [*Ardhuin et al.*, 2013, equation (16)]:

$$F_p(f_s) = \left[\rho_w (2\pi f_s)^2\right]^2 \int_{\partial V_e} dS \sum_{j=1}^{\infty} \left[\frac{\tan\left(l_j h\right)}{l_j}\right]^2 S_{DF,j}(f_s) \frac{e^{-\alpha_j(f_s)\Delta R_e}}{R_e \sin\Delta} \quad \text{(A5)}$$

with SI unit of Pa^2/Hz, in which l_j is the vertical wave number in water of mode j, h is the water depth. Here we shall take a constant group speed $U_j = 1800$ m s^{-1} and we absorb all variations of U_j in the empirical factor Q, whose mode dependence has been dropped. Thus, the exponential attenuation terms can be taken out of the sums over the modes in (A3) and (A5). In practice, we will use seven modes for our computations.

This formulation takes into account both the coupling with the ocean bottom and organ pipe modes via the site effect coefficient c_j, and the effect of remotely generated noise by integrating all contributions over the surface of the Earth (Stoneley waves only). All scattering and 3-D propagation effects in the crust and in the water are parameterized by a homogeneous isotropic frequency-dependent quality factor Q. The Earth's crust is usually modeled by a vertical stack of n homogeneous layers characterized by their densities, compressional and shear wave speeds, and thicknesses (all assumed constant). For simplicity, only one layer will be considered. The effects of an additional sediment layer are discussed in *Ardhuin et al.* [2013]. Its presence can especially affect the resonances in the water column and the transfer function from ocean surface to bottom. Stratification in the ocean is neglected as well but should be taken into account in a more realistic modeling [*Ying et al.*, 2014].

In (A3) and (A5), the space and time dependence of $E(f)$ and $I(f)$ has been dropped. If the attenuation is large compared to the noise relative variations, $E^2(f)I(f)$ can be considered as uniform and thus taken out of the surface integrals in (A3) and (A5). This will be particularly the case toward high frequencies, as it will be justified in section 3. Then we are left with a surface integral, which yields the attenuation length:

$$L_{\text{att}} = \int_{\partial V_e} dS \frac{e^{-\alpha(f_s)\Delta R_e}}{R_e \sin\Delta} = \frac{2\pi}{\alpha}\left[1 - e^{-\alpha\pi R_e}\right] \quad \text{(A6)}$$

since $dS = R_e^2 d\Delta \sin\Delta d\phi$, where ϕ is the azimuth of the source. Then the attenuation length becomes:

$$L_{\text{att}} \rightarrow \frac{2\pi}{\alpha} = \frac{UQ}{f_s} \quad \text{(A7)}$$

when $Q \rightarrow 0$ which is verified to a great extent by region 3 noise. This yields the definition in equation (10) of the transfer function γ from the surface equivalent pressure to the bottom pressure spectrum. In addition, it is implicitly assumed in equations (A3) and (A5) that seismic waves cannot travel around the earth and reach their source area again. Thus, an upper bound for L_{att} is $2\pi R_e$ typically. For $f_s = 1$ Hz, it yields a quality factor $Q = 22{,}000$ approximately.

Acknowledgments
Charles Peureux thanks the École Normale Supérieure de Lyon for financial support in the form of a fourth year study project. This work is supported by Agence Nationale de la Recherche grant ANR-14-CE01-0012 "MIMOSA" and by Labex Mer via grant ANR-10-LABX-19-01. William Farrell, Bertrand Chapron, and Michael Banner are greatly acknowledged for their valuable comments. We thank ECMWF for providing analyzed wind fields for this study. Data from the Cascadia array can be accessed at http://ds.iris.edu/gmap/7D. We thank IRIS for providing freely available data.

References

Abramovici, F. (1968), Diagnostic diagrams and transfer functions for oceanic wave-guides, *Bull. Seismol. Soc. Am.*, *58*(1), 427–456.
Ardhuin, F., and T. H. C. Herbers (2013), Noise generation in the solid earth, oceans and atmosphere, from nonlinear interacting surface gravity waves in finite depth, *J. Fluid Mech.*, *716*, 316–348, doi:10.1017/jfm.2012.548.
Ardhuin, F., and A. Roland (2012), Coastal wave reflection, directional spread, and seismoacoustic noise sources, *J. Geophys. Res.*, *117*, C00J20, doi:10.1029/2011JC007832.
Ardhuin, F., et al. (2010), Semiempirical dissipation source functions for ocean waves. Part i: Definition, calibration, and validation, *J. Phys. Oceanogr.*, *40*(9), 1917–1941, doi:10.1175/2010JPO4324.1.
Ardhuin, F., E. Stutzmann, M. Schimmel, and A. Mangeney (2011), Ocean wave sources of seismic noise, *J. Geophys. Res.*, *116*, C09004, doi:10.1029/2011JC006952.

Ardhuin, F., T. Lavanant, M. Obrebski, L. Marié, J.-Y. Royer, J.-F. d'Eu, B. M. Howe, R. Lukas, and J. Aucan (2013), A numerical model for ocean ultra-low frequency noise: Wave-generated acoustic-gravity and Rayleigh modes, *J. Acoust. Soc. Am.*, *134*(4), 3242–3260, doi:10.1121/1.4818840.
Ardhuin, F., L. Gualtieri, and E. Stutzmann (2015), How ocean waves rock the earth: Two mechanisms explain microseisms with periods 3 to 300 s, *Geophys. Res. Lett.*, *42*, 765–772, doi:10.1002/2014GL062782.
Bernard, P. (1941), Sur certaines proprits de la houle étudiées à l'aide des enregistrements seismographiques, *Bull. Inst. Oceanogr.*, *8*, 1–19, Monaco.
Bidlot, J.-R., et al. (2007), Inter-comparison of operational wave forecasting systems, paper presented at 10th International Workshop on Wave Hindcasting and Forecasting and Coastal Hazard Symposium, North Shore, Oahu, Hawaii.
Brekhovskikh, L. M. (1966), Underwater sound waves generated by surface waves in the ocean, *Izv. Acad. Sci. USSR Atmos. Oceanic Phys.*, *2*, 970–980.
Bromirski, P. D., F. K. Duennebier, and R. A. Stephen (2005), Mid-ocean microseisms, *Geochem. Geophys. Geosyst.*, *6*, Q04009, doi:10.1029/2004GC000768.
Cox, C. S., and D. C. Jacobs (1989), Cartesian diver observations of double frequency pressure fluctuations in the upper levels of the ocean, *Geophys. Res. Lett.*, *16*(8), 807–810, doi:10.1029/GL016i008p00807.
Duennebier, F. K., R. Lukas, E.-M. Nosal, J. Aucan, and R. A. Weller (2012), Wind, waves, and acoustic background levels at station aloha, *J. Geophys. Res.*, *117*, C03017, doi:10.1029/2011JC007267.
Elfouhaily, T., B. Chapron, K. Katsaros, and D. Vandemark (1997), A unified directional spectrum for long and short wind-driven waves, *J. Geophys. Res.*, *102*(C7), 15,781–15,796, doi:10.1029/97JC00467.
Farrell, W. E., and W. Munk (2008), What do deep sea pressure fluctuations tell about short surface waves?, *Geophys. Res. Lett.*, *35*, L19605, doi:10.1029/2008GL035008.
Farrell, W. E., and W. Munk (2010), Booms and busts in the deep, *J. Phys. Oceanogr.*, *40*(9), 2159–2169, doi:10.1175/2010JPO4440.1.
Farrell, W. E., and W. Munk (2013), Surface gravity waves and their acoustic signatures, 1-30 hz, on the mid-pacific sea floor, *J. Acoust. Soc. Am.*, *134*(4), 3134, doi:10.1121/1.4818780.
Gimbert, F., and V. C. Tsai (2015), Predicting short-period, wind-wave-generated seismic noise in coastal regions, *Earth Planet. Sci. Lett.*, *426*, 280–292, doi:10.1016/j.epsl.2015.06.017.
Gualtieri, L., E. Stutzmann, V. Farra, Y. Capdeville, M. Schimmel, F. Ardhuin, and A. Morelli (2014), Modelling the ocean site effect on seismic noise body waves, *Geophys. J. Int.*, *197*(2), 1096–1106, doi:10.1093/gji/ggu042.
Gualtieri, L., E. Stutzmann, Y. Capdeville, V. Farra, A. Mangeney, and A. Morelli (2015), On the shaping factors of the secondary microseismic wavefield, *J. Geophys. Res. Solid Earth*, *120*, 6241–6262, doi:10.1002/2015JB012157.
Guralnik, Z., J. Bourdelais, X. Zabalgogeazcoa, and W. E. Farrell (2013), Wave-wave interactions and deep ocean acoustics, *J. Acoust. Soc. Am.*, *134*(4), 3161, doi:10.1121/1.4818782.
Hasselmann, K. (1963), A statistical analysis of the generation of microseisms, *Rev. Geophys.*, *1*(2), 177–210, doi:10.1029/RG001i002p00177.
Hughes, B. (1976), Estimates of underwater sound (and infrasound) produced by nonlinearly interacting ocean waves, *J. Acoust. Soc. Am.*, *60*(5), 1032, doi:10.1121/1.381203.
Korotkevich, A. O. (2008), On the Doppler distortion of the sea-wave spectra, *Physica D*, *237*(21), 2767–2776.
Kudryavtsev, V., D. Akimov, J. Johannessen, and B. Chapron (2005), On radar imaging of current features: 1. Model and comparison with observations, *J. Geophys. Res.*, *110*, C07016, doi:10.1029/2004JC002505.
Latham, G. V., R. S. Anderson, and M. Ewing (1967), Pressure variations produced at the ocean bottom by hurricanes, *J. Geophys. Res.*, *72*(22), 5693–5704, doi:10.1029/JZ072i022p05693.
Leckler, F., F. Ardhuin, C. Peureux, A. Benetazzo, F. Bergamasco, and V. Dulov (2015), Analysis and interpretation of frequency-wavenumber spectra of young wind waves, *J. Phys. Oceanogr.*, *45*(10), 2484–2496, doi:10.1175/JPO-D-14-0237.1.
Longuet-Higgins, M. S. (1950), A theory of the origin of microseisms, *Philos. Trans. R. Soc. London A*, *243*(857), 1–35, doi:10.1098/rsta.1950.0012.
Longuet-Higgins, M. S., and R. W. Stewart (1961), The changes in amplitude of short gravity waves on steady non-uniform currents, *J. Fluid Mech.*, *10*(04), 529–549, doi:10.1017/S0022112061000342.
McCreery, C. S. (1993), Correlation of deep ocean noise (0.4-30 hz) with wind, and the Holu spectrum—A worldwide constant, *J. Acoust. Soc. Am.*, *93*(5), 2639, doi:10.1121/1.405838.
McCreery, C. S., and F. K. Duennebier (1988), The Holu spectrum: A worldwide deep-ocean constant, and indicator of the ocean wave spectrum, *Eos Trans. AGU*, *69*, 1245.
Nan, Q. L., A. Prosperetti, and S. W. Yoon (1990), Underwater noise emissions from bubble clouds, *IEEE J. Oceanic Eng.*, *15*(4), 275–281, doi:10.1109/48.103521.
Neale, J., N. Harmon, and M. Srokosz (2015), Source regions and reflection of infragravity waves offshore of U.S.'s Pacific northwest, *J. Geophys. Res. Oceans*, *120*, 6474–6491, doi:10.1002/2015JC010891.
Phillips, O. M. (1958), The equilibrium range in the spectrum of wind-generated waves, *J. Fluid Mech.*, *4*(04), 426–434, doi:10.1017/s0022112058000550.
Pierson, W. J., and L. Moskowitz (1964), A proposed spectral form for fully developed wind seas based on the similarity theory of S. A. Kitaigorodskii, *J. Geophys. Res.*, *69*(24), 5181–5190, doi:10.1029/JZ069i024p05181.
Rascle, N., and F. Ardhuin (2013), A global wave parameter database for geophysical applications. Part 2: Model validation with improved source term parameterization, *Ocean Modell.*, *70*, 174–188, doi:10.1016/j.ocemod.2012.12.001.
Rawat, A., F. Ardhuin, V. Ballu, W. Crawford, C. Corela, and J. Aucan (2014), Infragravity waves across the oceans, *Geophys. Res. Lett.*, *41*, 7957–7963, doi:10.1002/2014GL061604.
Stutzmann, E., F. Ardhuin, M. Schimmel, A. Mangeney, and G. Patau (2012), Modelling long-term seismic noise in various environments, *Geophys. J. Int.*, *191*(2), 707–722, doi:10.1111/j.1365-246x.2012.05638.x.
Tolman, H. L. (2014), *User Manual and System Documentation of WAVEWATCH-III TM, Version 4.18*, NOAA/NWS/NCEP/MMAB, 5830 University, Research Court, College Park, MD 20740.
Toomey, D., et al. (2014), The Cascadia initiative: A sea change in seismological studies of subduction zones, *Oceanography*, *27*(2), 138–150, doi:10.5670/oceanog.2014.49.
Webb, S. C. (1992), The equilibrium oceanic microseism spectrum, *J. Acoust. Soc. Am.*, *92*(4), 2141, doi:10.1121/1.405226.
Ying, Y., C. J. Bean, and P. D. Bromirski (2014), Propagation of microseisms from the deep ocean to land, *Geophys. Res. Lett.*, *41*, 6374–6379, doi:10.1002/2014GL060979.
Yurovskaya, M. V., V. A. Dulov, B. Chapron, and V. N. Kudryavtsev (2013), Directional short wind wave spectra derived from the sea surface photography, *J. Geophys. Res. Oceans*, *118*, 4380–4394, doi:10.1002/jgrc.20296.